



Efficient Spiking Point Mamba for Point Cloud Analysis

Peixi Wu¹, Bosong Chai², Menghua Zheng³, Wei Li¹, Zhangchi Hu¹,
Jie Chen¹, Zheyu Zhang¹, Hebei Li^{1*}, Xiaoyan Sun^{1*}

¹University of Science and Technology of China

²Zhejiang University ³Tsingmao Intelligence

{wupeixi, lihebei, sunxiaoyan}@ustc.edu.cn

Abstract

Bio-inspired Spiking Neural Networks (SNNs) provide an energy-efficient way to extract 3D spatio-temporal features. However, existing 3D SNNs have struggled with long-range dependencies until the recent emergence of Mamba, which offers superior computational efficiency and sequence modeling capability. In this work, we propose Spiking Point Mamba (SPM), the first Mamba-based SNN in the 3D domain. Due to the poor performance of simply transferring Mamba to 3D SNNs, SPM is designed to utilize both the sequence modeling capabilities of Mamba and the temporal feature extraction of SNNs. Specifically, we first introduce Hierarchical Dynamic Encoding (HDE), an improved direct encoding method that effectively introduces dynamic temporal mechanism, thereby facilitating temporal interactions. Then, we propose a Spiking Mamba Block (SMB), which builds upon Mamba while learning inter-time-step features and minimizing information loss caused by spikes. Finally, to further enhance model performance, we adopt an asymmetric SNN-ANN architecture for spike-based pre-training and finetune. Compared with the previous state-of-the-art SNN models, SPM improves OA by +6.2%, +6.1%, and +7.4% on three variants of ScanObjectNN, and boosts instance mIOU by +1.9% on ShapeNet-Part. Meanwhile, its energy consumption is at least 3.5× lower than that of its ANN counterpart.

1. Introduction

Bio-inspired Spiking Neural Networks (SNNs) offer a promising energy-efficient paradigm for 3D point cloud analysis, leveraging event-driven computation and intrinsic spatio-temporal dynamics [43, 44]. Despite recent advances in MLP-based and Transformer-based SNN archi-

*Corresponding authors.

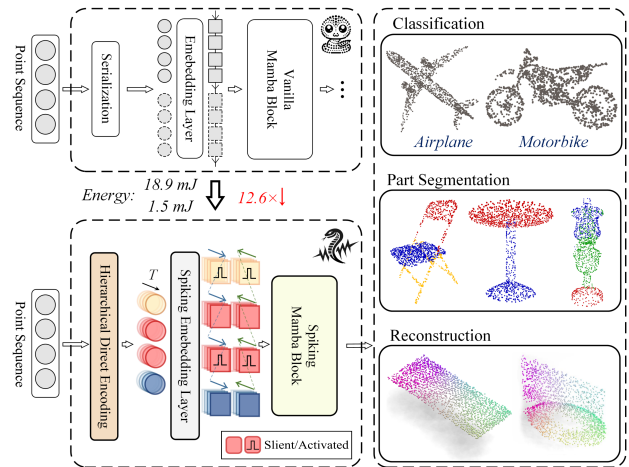


Figure 1. The SNN-adapted design of Spiking Point Mamba, compared to PointMamba [24], serves as an efficient backbone for various 3D point cloud analysis tasks, including object classification, part segmentation, and reconstruction.

tures [41, 42, 53], critical limitations persist: (1) Existing models struggle to capture long-range dependencies (LRDs) in irregular point sequences; (2) Static temporal encoding methods [35, 68] fail to exploit the dynamic nature of spike-driven temporal features; (3) Information degradation during spike-driven computation remains unaddressed [67], particularly when integrating modern sequence modeling techniques.

The recent success of Mamba architectures in 3D vision [18, 24] provides new opportunities. Their selective state space mechanisms enable more effective LRD modeling [11]. However, naively adapting Mamba to SNNs faces two challenges: (1) Temporal complexity mismatch between continuous state transitions and discrete spike events, and (2) Information density disparity (30% fewer activations per timestep compared to ANNs [66, 67]).

To bridge this gap, we propose Spiking Point Mamba (SPM), the first Mamba-based SNN framework that synergizes energy-efficient spike computation with powerful sequence modeling. First, we introduce an improved direct encoding called Hierarchical Dynamic Encoding (HDE) to SPM. Most of the high-performance SNN studies [35, 41, 68] are based on direct encoding, repeating the input along the time dimension to generate a static encoding sequence. However, it fails to fully exploit the potential of SNNs in extracting the temporal feature effectively [60, 64]. To this end, HDE introduces dynamics in the early unstable and late redundant stages of farthest point sampling (FPS) while preserving the key information at each time step in the middle stage. HDE transforms the static point cloud into a hierarchical, dynamic event-based representation, facilitating better feature interaction in SPM.

Then, we propose Spiking Mamba Block (SMB) as the core component of SPM to leverage the capacity of both Mamba and SNNs. Although Mamba demonstrates strong performance in sequence modeling [5, 11], its original architecture is not fully compatible with the spike-based input [46, 66]. To this end, we customize the Gate branch and the SSM feature extraction branch of SMB. The design not only preserves the modeling capacity of Mamba, but also enhances the dynamic interactions across time steps while minimizing the information loss caused by spike. To boost the performance of SPM across various datasets and tasks, we pretrain SPM through a heterogeneous SNN-ANN architecture, effectively leveraging the modeling strengths of 3D ANNs to enhance the generalization of SPM.

In summary, our main contributions are as follows:

- We build Spiking Point Mamba (SPM), the first energy-efficient Mamba-based 3D SNN framework, and introduce spike-based pre-training to the 3D SNN domain.
- We propose Hierarchical Dynamic Encoding (HDE), an improved direct encoding method that enhances temporal interactions via dynamic temporal mechanism.
- We introduce Spiking Mamba Block (SMB), which builds upon the modeling capabilities of Mamba while learning features across time steps effectively.
- Extensive experimental results demonstrate that SPM achieves significant performance improvements in various downstream tasks.

2. Related Works

State Space Models. Inspired by continuous state space models in control systems, recent research has shown that SSM [8, 32], as a promising alternative to sequence models such as RNNs and Transformers, can effectively model LRDs. To maintain performance while reducing computational costs, HTTYH [15], DSS [17], and S4D [14] propose using diagonal matrices within S4 [13]. S5 [48] introduce parallel scanning and MIMO SSM. Recently, Mamba [12]

introduces the selective SSM mechanism, achieving linear-time inference and efficient training. Meanwhile, various variants of SSMs [34] have been successfully applied to many domains involving audio [6, 10], video [22, 57] and vision [28, 33, 69].

Deep Learning for Point Cloud. Point cloud analysis follows two main approaches: projecting raw point clouds onto voxel grids or images [23, 31, 47], and directly processing raw point cloud. The success of transformers in deep learning has driven a shift from MLP-based [30, 39, 40] to transformer-based methods [37, 53, 55], but their quadratic complexity increases computational costs, posing challenges for long-sequence point clouds. Recently, Mamba has emerged as a more efficient alternative with linear complexity and strong sequence modeling [22, 69]. By effectively capturing long-range dependencies (LRDs), Mamba-based methods [24, 26, 27, 62, 65] provide a more efficient and scalable solutions for point cloud analysis.

SNN Training and Architecture Design. The primary challenge in training SNNs is the non-differentiable spike function [41]. To address this, recent research focuses on improving training strategies and architectures. Some studies [2, 19] concentrate on ANN-to-SNN conversion [20, 50], which transforms trained ANNs into equivalent SNNs using neuron equivalence. However, this approach requires long time steps and increases energy consumption. Alternatively, other works directly train SNNs using surrogate gradients [16], striving to make computations spike-driven as much as possible [58], thereby enabling low energy use and high performance with shorter time steps. Our architecture follows this direct training paradigm.

3. Preliminaries

3.1. LIF Neuron

The Leaky Integrate-and-Fire (LIF) neuron, a simplified biological neuron model, captures the "leaky-integrate-fire-reset" process [45]. It is the most popular neuron due to its balance of bio-plausibility and computing complexity. Given time step t , the LIF neuron is formulated by following equations:

$$\mathbf{H}_t = f(\mathbf{V}_{t-1}, \mathbf{X}_t) \quad (1)$$

$$\mathbf{S}_t = \Theta(\mathbf{H}_t - V_{th}) \quad (2)$$

$$\mathbf{V}_t = \mathbf{H}_t \cdot (1 - \mathbf{S}_t) + V_r \cdot \mathbf{S}_t \quad (3)$$

where \mathbf{H}_t and \mathbf{V}_t are defined as the membrane potential after neuronal dynamics and after spike triggering, with \mathbf{X}_t as the external input and V_{th} as the firing threshold. The output spike \mathbf{S}_t follows Eq. (2), where $\Theta(\cdot)$ denotes the Heaviside function. After firing, \mathbf{V}_t resets to V_r as shown in Eq. (3), while Eq. (1) models the leaky-integrate process, where $f(\cdot)$ governs decay and input accumulation. We uniformly adopt the LIF neuron for \mathcal{SN} in the following sections.

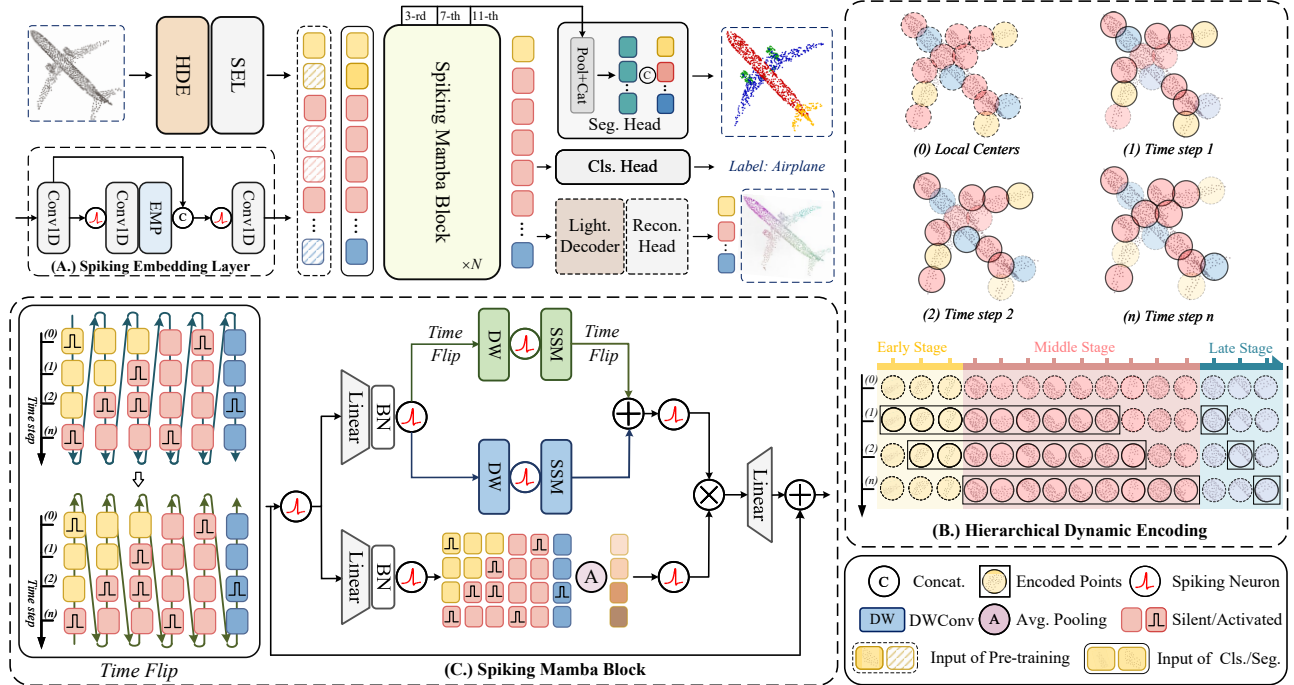


Figure 2. The overview of Spiking Point Mamba (SPM), which consists of Hierarchical Dynamic Encoding (HDE), Spiking Embedding Layer (SEL) for adaptive learning, Spiking Mamba Block (SMB) for feature interaction. For downstream tasks, we design Classification and Segmentation Head, while for pre-training, we design Reconstruction Head with a lightweight decoder.

3.2. State Space Model

Drawing inspiration from control theory, the State Space Model (SSM) represents a continuous system that maps an input state \mathbf{x} to an output \mathbf{y} through an implicit latent state \mathbf{h} . For a discrete input sequence $\mathbf{x}_{1:L}$, through certain discretization rule the SSMs can be defined by:

$$\mathbf{h}_k = \bar{\mathbf{A}}\mathbf{h}_{k-1} + \bar{\mathbf{B}}\mathbf{x}_k \quad (4)$$

$$\mathbf{y}_k = \mathbf{C}\mathbf{h}_k + \mathbf{D}\mathbf{x}_k \quad (5)$$

where \mathbf{C} is a projection parameter, and \mathbf{D} is a residual connection. The parameters $\bar{\mathbf{A}}$ and $\bar{\mathbf{B}}$ are discretized using the zero-order hold (ZOH) rule, introducing the timescale parameter Δ . The SSMs are applied separately to each channel with data-independent parameters, limiting flexibility in sequence modeling. Recently, Mamba introduces the selective SSM, where $\bar{\mathbf{B}}$, $\bar{\mathbf{C}}$, and Δ depend on the input, improving the sequence modeling. In the following sections, both SSM and Mamba refer to the S6 model.

4. Method

4.1. Main Architecture

We propose Spiking Point Mamba (SPM), the first Spiking Neuron Network framework based on Mamba architecture, as shown in Fig. 2. First, Hierarchical Dynamic Encoding

(HDE) is applied to the point cloud for time-dynamic encoding, generating tokenized representations. These tokens are then mapped to semantic features via Spiking Embedding Layer (SEL). Spiking Mamba Block (SMB) further models both inter-token and inter-time-step interactions. Finally, the output is passed to different heads for various downstream tasks.

4.1.1. Hierarchical Dynamic Encoding

Most SNN studies rely on direct encoding by repeating the input along the time dimension, limiting the temporal feature extraction due to its static nature. We introduce Hierarchical Dynamic Encoding (HDE), which treats each time step as richer input, introducing temporal dynamics. However, given the temporal correlation of neurons, it is essential to preserve key information at each time step while introducing dynamic changes to avoid distortion.

Meanwhile, considering the characteristics of farthest point sampling (FPS), it can be divided into three stages: early, middle, and late. The early stage is unstable primarily due to the random initial selection, and the middle stage stabilizes effectively capturing the skeletal structure of the point cloud, while the late stage may introduce redundancy or noise because of the sufficient sampling, as further validated in Appendix A. Hence, we process these three stages hierarchically to introduce dynamic changes.

As shown in Algorithm 1, HDE first downsamples the original point set \mathbf{P} to obtain the sampled set \mathbf{S} , which is then divided into three stages: early, middle, and late, with L , M , and R points respectively. In the early and middle stages, we dynamically select F points from \mathbf{S} using a shifting sampling strategy with a step size of l . This dynamic mechanism ensures diversity in the initial sampling distribution while retaining key structural information. Due to the instability of randomly selected initial points within a limited range, L remains constant, while l decreases with time, referred to as *Finite Forward Sliding*. In the late stage, r points are dynamically selected from the remaining R points as a memory pool for each time step, referred to as *Infinite Backward Extension*, where R increases with time, while r remains constant. Finally, the point sets from *Finite Forward Sliding* and *Infinite Backward Extension* are merged to generate the encoded point matrix \mathbf{E} . Together, the entire HDE process is observed in Fig. 2.

4.1.2. Spiking Embedding Layer

After Hierarchical Dynamic Encoding (HDE), the K-Nearest Neighbors (KNN) algorithm is applied to each encoded center point to find its K nearest neighbors, treated as tokens \mathbf{T} . These tokens are then mapped by Spiking Embedding Layer (SEL) to obtain higher-dimensional semantic features, which are further processed by SMB.

Specifically, SEL projects the tokens to derive the membrane potential \mathbf{U} with preliminary learned deeper semantic information. Subsequently, an element-wise MaxPooling (EMP) is applied across all tokens to capture the local context of each token, which is then concatenated with \mathbf{U} as an additional feature. This combined representation is further processed through a series of fully connected layers and spiking neurons to obtain the final embedded feature membrane potential \mathbf{U}' . Finally, the entire representation is obtained by adding the potential with its positional embedding. Together, SEL can be formulated as:

$$\mathbf{U} = \text{MLP}(\mathcal{N}(\text{MLP}(\mathbf{T}))) \quad (6)$$

$$\mathbf{G} = \text{EMP}(\mathbf{U}), \text{RPE} = \text{MLP}(\mathbf{E}) \quad (7)$$

$$\mathbf{U}' = \text{MLP}(\mathcal{N}(\text{Concat}(\mathbf{U}, \mathbf{G}))) \quad (8)$$

$$\mathbf{U}_0 = \mathbf{U}' + \text{RPE} \quad (9)$$

where MLP is composed of a conv layer and a batch normalization layer. RPE means relative position embedding. \mathbf{T} and \mathbf{U}_0 are features in $\mathbb{R}^{T \times E \times K \times C}$ and $\mathbb{R}^{T \times E \times C'}$, representing the tokens indexing based on KNN from \mathbf{E} and the final output of SEL respectively.

4.1.3. Spiking Mamba Block

Spiking Mamba Block (SMB) is the core component of the Spiking Point Mamba (SPM), integrating the strengths of both Mamba and SNNs. SMB processes both the temporal dynamics introduced by HDE and the interactions be-

Algorithm 1 Hierarchical Dynamic Encoding

```

1: Result: Encoded point matrix  $\mathbf{E} \in \mathbb{R}^{T \times E \times C}$ 
2: Input: Point set  $\mathbf{P}$ , Sampled Points  $S$ , Time Step  $T$ 
3:       Early Stage  $L$ , Mid Stage  $M$ , Late Stage  $R$ 
4: # Sampling
5:  $\mathbf{S} \leftarrow \text{FPS}(\mathbf{P}, S)$ 
6: # Encoding
7:  $l = \lfloor L/T \rfloor, r = \lfloor R/T \rfloor$ 
8:  $M \leftarrow M + L, F \leftarrow E - r$ 
9: for  $i = 1, 2, 3, \dots, T$  do
10:   # Finite Forward Sliding
11:    $\mathbf{F}_i \leftarrow \{s_j \mid i \cdot l \leq j < F + i \cdot l\}$ 
12:   # Infinite Backward Extension
13:    $\mathbf{B}_i \leftarrow \{s_j \mid M + i \cdot r \leq j < M + (i + 1) \cdot r\}$ 
14:    $\mathbf{E}_i \leftarrow \mathbf{F}_i \cup \mathbf{B}_i$ 
15: end for

```

tween membrane potential tokens. Similar to previous research, Spiking Point Mamba iteratively applies the SMB N times, refining the input membrane potential \mathbf{U}_0 at each block. The output of each SMB is defined as \mathbf{U}_n .

Specifically, \mathbf{U}_n is first processed by a spiking neuron to generate spike \mathbf{S}_n , enabling sparse synaptic accumulation in subsequent operations. SMB consists of two branches: SSM branch and Gate branch. For SSM branch, it first encodes \mathbf{S}_n with fully connected layers and neurons to extract the intermediate feature spike \mathbf{S}'_n . Unlike previous works, reversing the token dimension in \mathbf{S}'_n is not meaningful, as it is a sparse spike matrix with less information. Instead, we reverse only the time dimension to help SSM branch learn dynamic relationships between time steps. After timestep-wise interactions, \mathbf{S}''_n is obtained through a spiking neuron. For Gate branch, it first maps \mathbf{S}_n to a higher dimension to generate a gating matrix \mathbf{Z}_n . However, element-wise multiplication between \mathbf{Z}_n and \mathbf{S}''_n leads to significant information loss and disrupts token relationships. To address this, we apply element-wise average pooling (EAP) on \mathbf{Z}_n along the token dimension, preserving important feature dimensions while maintaining token relationships. Finally, \mathbf{U}_{n+1} is obtained through a linear layer and residual connection. Together, SMB can be formulated as:

$$\mathbf{S}_n = \mathcal{N}(\mathbf{U}_n) \quad (10)$$

$$\mathbf{S}'_n = \mathcal{N}(\text{MLP}(\mathbf{S}_n)) \mathbf{Z}_n = \mathcal{N}(\text{MLP}(\mathbf{S}_n)) \quad (11)$$

$$\mathbf{U}'_n, \mathbf{U}'_t = \text{SSM}(\mathcal{N}(\text{DWConv}(\mathbf{S}'_n, \mathbf{S}'_t))) \quad (12)$$

$$\mathbf{S}''_n = \mathcal{N}(\mathbf{U}'_n + \mathbf{U}'_t) \circ \mathcal{N}(\text{EAP}(\mathbf{Z}_n)) \quad (13)$$

$$\mathbf{U}_{n+1} = \text{MLP}(\mathbf{S}''_n) + \mathbf{U}_n \quad (14)$$

where \mathbf{S}'_t and \mathbf{U}'_t represent the time dimension reversal of \mathbf{S}'_n and its output through the SSM module, while \circ denotes the Hadamard product between the spike tensors. $n = 1, 2, \dots, N$ represents the layer number.

4.2. Spike-based Pre-training Modeling

Inspired by the success of pre-training in 2D SNNs, we introduce a masked modeling pre-training framework into 3D SNNs for robust point cloud feature representations, as shown in Fig. 2. A key challenge is to maximize the effectiveness of spike-based pre-training. To this end, we utilize an asymmetric SNN-ANN heterogeneous encoder-decoder architecture based on SMB and Mamba Block.

Specifically, the encoder consists of N stacked SMBs, while the decoder utilizes a unidirectional SSM that is stacked N_d times for lightweight ANN decoding, where $N_d < N$. This design preserves the asymmetry between the encoder and decoder, accelerating the pre-training. It also decouples SNN and ANN, leveraging the ANN decoder’s modeling capability to enhance the SNN encoder’s representation capacity while ensuring low energy consumption during inference. Chamfer Distance is used as the reconstruction loss to recover the original point cloud. Together, the spike-based pre-training modeling can be formulated as follows:

$$\mathbf{T}'_v = \mathcal{E}_{\text{SMB}}(\mathbf{T}_v) \quad (15)$$

$$\mathbf{H}_v, \mathbf{H}_m = \mathcal{D}_{\text{SSM}}(\mathbf{T}'_v, \mathbf{T}_m) \quad (16)$$

$$\mathbf{P}_m = \mathcal{H}(\mathbf{H}_m) \quad (17)$$

where \mathbf{T}_v and \mathbf{T}_m denote the visible and masked tokens after token masking, respectively, while \mathbf{T}'_v represents the encoded features of the visible tokens. \mathbf{H}_v and \mathbf{H}_m are the decoded features. \mathbf{P}_m denotes the reconstructed point cloud. \mathcal{E}_{SMB} and \mathcal{D}_{SSM} represent the encoder stacked with SMB and decoder stacked with SSM, respectively, and \mathcal{H} is the reconstruction head.

4.3. Theoretical Energy Consumption

In this section, we investigate energy efficiency of our SPM architecture. SPM converts matrix multiplication into sparse addition. Specifically, unlike ANNs where almost all FLOPs are multiply-accumulate (MAC) operations, SNNs use sparse spikes with only a subset of neurons activated for sparse accumulation (AC). According to the research [1], a 32-bit floating-point consumes $4.6pJ$ for a MAC operation and $0.9pJ$ for an AC operation, namely $E_{\text{MAC}} = 4.6pJ$ and $E_{\text{AC}} = 0.9pJ$.

The energy consumption of SPM primarily involves SEL and SMB. The SEL module consists of the initial floating-point MAC operations and the subsequent spike-based synaptic accumulation operations. The energy consumption can be expressed as:

$$E_{\text{SEL}} = E_{\text{MAC}} \cdot FL_{\text{conv}}^{\mathbf{T}, \mathbf{E}} + E_{\text{AC}} \cdot FL_{\text{conv}}^{\mathbf{U}, \mathbf{G}} \cdot T \cdot f_{\text{conv}}^{\mathbf{U}, \mathbf{G}} \quad (18)$$

where $f_{\text{conv}}^{\mathbf{U}, \mathbf{G}}$ represent the firing rates of \mathbf{U}, \mathbf{G} after $\mathcal{S}\mathcal{N}$, while $FL_{\text{conv}}^{\mathbf{T}, \mathbf{E}}, FL_{\text{conv}}^{\mathbf{U}, \mathbf{G}}$ denote the FLOPs of corresponding conv layers of $\mathbf{T}, \mathbf{E}, \mathbf{U}$ and \mathbf{G} .

In the SMB module, all conv layers transmit spikes and performs AC operations, ensuring efficient and event-driven processing. SSM involves most AC operations with a small number of MAC operations introduced due to the floating-point multiplications between \mathbf{A}, \mathbf{C} , and hidden state \mathbf{h} . The energy consumption can be given by:

$$E_{\text{SSM}} = E_{\text{MAC}} \cdot FL_1^n + E_{\text{AC}} \cdot FL_2^n \cdot T \cdot f_2^n \quad (19)$$

$$E_{\text{SMB}} = E_{\text{SSM}} + E_{\text{AC}} \cdot FL_{\text{conv}}^n \cdot T \cdot f_{\text{conv}}^n \quad (20)$$

where f_{conv}^n and f_2^n denote the firing rates of the input spikes to different conv layers and SSM in n -th SMB respectively. $FL_{\text{conv}}^n, FL_1^n$ and FL_2^n represent the FLOPs of different conv layers, floating-point multiplication, and spike-based multiplication in n -th SSM respectively. T represents the time step.

5. Experiments

5.1. Experimental Settings

5.1.1. Datasets

We evaluate the performance of 3D point cloud classification on the synthetic dataset ModelNet40 [56] and the real dataset ScanObjectNN [49]. ModelNet40 contains 40 different object categories, each of which contains a large number of 3D object instances. ScanObjectNN contains 2902 point clouds from 15 categories. It is a more challenging dataset sampled from real world scans. We follow previous works to conduct experiments on three main variants: OBJ-BG, OBJ-ONLY and PB-T50-RS.

We also evaluate our proposed SPM on the part segmentation dataset ShapeNetPart [59], which includes 16,881 models across 16 categories. For pre-training experiments, we utilize ShapeNet [4], a comprehensive dataset containing over 50,000 unique 3D models from 55 common object categories, ensuring robust feature learning.

5.1.2. Implementation Details

For classification experiments, the number of input points is set to 2048 by default, adjusted to 1024 for ModelNet40. After HDE, the number of points per time step E , is set to 256, or 128 for ModelNet40. The number of points in the early or late stage is $10\%E$. The layer number of Spiking Mamba Block N is 12. For most neurons, V_{th} is set to 0.5 while for neurons before each SSM, V_{th} is set to 0.25. For segmentation experiments, we utilize the same backbone as in classification experiments. For pre-training experiments, the mask ratio is set to 0.6. For fine-tuning experiments, the training epochs is halved to improve training efficiency.

In most experiments, we utilize the AdamW optimizer and conduct 300 epochs of iterative training on $2 \times \text{RTX } 4090$ GPUs. The remaining hyperparameters are consistent with previous research [18, 24] for fair comparison. More experimental details can be found in Appendix C.

Architecture	Methods	Params	T	ScanObjectNN			ModelNet40	
				OBJ-BG	OBJ-ONLY	PB-T50-RS	w/o Vote	w/ Vote
ANN	PointNet [39]	3.5	-	73.3	79.2	68.0	89.2	-
	PointNet++ [40]	1.5	-	82.3	84.3	77.9	90.7	-
	PointMLP [30]	13.2	-	-	-	85.4	94.1	94.5
	PointMamba [24]	12.3	-	90.2*	89.8*	85.4	92.4	-
SNN	KPConv-SNN [54]	-	40	-	-	70.5	-	43.9
	Spiking Pointnet [42]	3.5	4	72.2*	76.4*	64.1	88.2	88.8
	SpikingPointNet [21]	3.5	16	-	-	69.2	88.6	-
	P2SResLNet-B [54]	14.3	1	78.6*	80.2*	74.5	-	88.7
	Spiking Point Transformer [52]	10.2	4	82.8*	83.4*	78.0	91.4	91.6*
	Spiking Point Mamba (Ours)	12.8	4	90.2(↑ 7.4)	89.5(↑ 6.1)	84.2(↑ 6.2)	92.3(↑ 0.9)	92.7(↑ 1.1)

Table 1. Performance comparison with the baseline methods. We report overall accuracy (%) on three ScanObjectNN variants and on ModelNet40 with and without voting. The best results in the SNN domain are bolded, with * and ↑ indicating self-reproduced results and the improvement compared to Spiking Point Transformer.

Architecture	Methods	PB-T50-RS	ModelNet40
ANN	Point-BERT [61]	83.1	92.7
	MaskPoint [25]	84.3	93.8
	Point-MAE [36]	85.2	93.2
	Point-M2AE [63]	86.4	93.4
	PointMamba [24]	88.2	93.6
SNN	SPT[52]*	82.6	92.5
	SPM (Ours)	86.5(↑ 3.9)	93.1(↑ 1.4)

Table 2. Performance of self-supervised learning methods. We report overall accuracy (%) on PB-T50-RS and ModelNet40.

Architecture	Methods	Cls. mIoU	Ins. mIoU
ANN	PointNet [39]	80.39	83.7
	PointNet++ [40]	81.85	85.1
	DGCNN [38]	82.33	85.2
	APES [51]	83.67	85.8
	PointMamba [24]	84.29	85.8
SNN	SPT[52]*	81.32	82.9
	SPM (Ours)	82.29(↑ 0.97)	84.8(↑ 1.9)

Table 3. Performance of part segmentation methods. We report Cls. mIoU (%) and Ins. mIoU (%) on ShapeNetPart.

5.2. Experimental Results

5.2.1. Object Classification

We compare SPM with other state-of-the-art methods on OBJ-BG, OBJ-ONLY, PB-T50-RS and ModelNet40 datasets and report the results in Tab. 1 and Tab. 2. All the methods we compare are based on LIF, which is the most popular neuron. Moreover, we use Overall Accuracy (OA) to evaluate the classification performance of all methods.

As shown in Tab. 1, our proposed SPM achieves the state-of-the-art performance in the SNN domain on both ScanObjectNN and ModelNet40 datasets, significantly outperforming SNN baselines. Specifically, on the PB-T50-RS, OBJ-ONLY, and OBJ-BG subsets, SPM attains 84.2%, 89.5%, and 90.2% OA, surpassing SPT by 6.2%, 6.1%, and 7.4%, respectively. Moreover, on the ModelNet40 dataset, SPM achieves 92.3% OA, reflecting a 0.9% improvement over SPT. This means that the introduction of Mamba enhances SPM’s sequence modeling capabilities. In the ANN domain, SPM performs comparably to PointMamba, confirming that SPM benefits not only from Mamba but also from the temporal feature extraction of SNN.

As shown in Tab. 2, we also evaluate the performance of spike-based pre-training model for SPM using two representative datasets: PB-T50-RS and ModelNet40. In the SNN domain, our SPM achieves the state-of-the-art performance and outperforms SPT with 86.5% OA on PB-T50-RS and 93.1% OA on ModelNet40. In addition, compared to training from scratch on PB-T50-RS and ModelNet40, SPM shows an improvement of 2.3%, and 0.8% respectively. In the ANN domain, SPM performs nearly on par with Point-M2AE. These results illustrate that spike-based pre-training effectively enhances the SNN encoder.

5.2.2. Part Segmentation

We further evaluate SPM on the ShapeNetPart dataset using two metrics: Cls. mIoU and Ins. mIoU, which measure the mean intersection over union for categories and instances, respectively. As shown in Tab. 3, SPM demonstrates superior performance within the SNN domain, achieving 82.29% Cls. mIoU and 84.8% Ins. mIoU, surpassing SPT by 0.97% and 1.9%, respectively. In the ANN domain, while SPM slightly lags behind PointMamba in mIoU, it offers a compelling balance between performance and energy efficiency as further illustrated in Tab. 7.

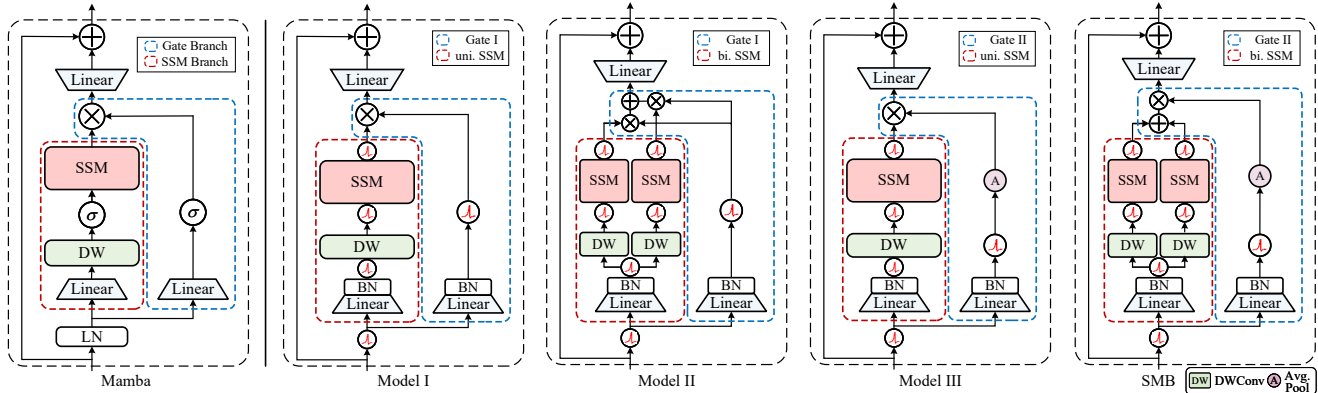


Figure 3. Ablation study of the design of SMB. Model I-III denote three variant models of SMB while Mamba denotes ANN counterpart. Gate I and Gate II represent vanilla and SNN-adapted Gate Branch. uni. and bi. SSM represent unidirectional and directional SSM.

Architecture	Models	Gate Branch		SSM Branch		ScanObjectNN			ModelNet40
		Gate I	Gate II	bi.	uni.	OBJ-BG	OBJ-ONLY	PB-T50-RS	
ANN	Mamba	-	-	-	-	90.2	89.5	84.2	92.3
SNN	Model I	✓	✗	✗	✓	88.3	87.9	83.1	91.4
	Model II	✓	✗	✓	✗	89.3	88.9	83.8	91.8
	Model III	✗	✓	✗	✓	88.9	88.4	83.5	91.6
	SMB	✗	✓	✓	✗	90.2	89.5	84.2	92.3

Table 4. Ablation study of the design of SMB. We report overall accuracy (%) on three ScanObjectNN variants and ModelNet40.

5.3. Ablation Studies

To analyze each module in SPM, we conduct a series of ablative experiments on ScanObjectNN and ModelNet40 datasets. We construct three variants Model I-III, which correspond to the ablation of our proposed improvements in two branches. Furthermore, we conduct ablation studies on the bidirectional strategy, input encoding and time step.

5.3.1. Ablation on SMB

Our proposed SMB enhances both Gate and SSM branches of Mamba. Therefore, we conduct ablation studies on them, constructing three variant models (Model I-III) as shown in Fig. 3. Additionally, we conduct a more detailed ablation on the bidirectional strategy of the SSM branch.

Branch Architecture Fig. 3 shows how SPM enhances Mamba’s gating and SSM branches for better adaptation to SNNs. Specifically, Gate I merely replaces ReLU/SiLU with LIF, while Gate II minimizes information loss from spike gating. The uni. and bi. refer to unidirectional and bidirectional SSM branches. From Tab. 4, we observe that SPM outperforms Models I-III. Compared to Model I, SPM achieves improvements of 1.9%, 1.6%, 1.1%, and 0.9% OA on OBJ-BG, OBJ-ONLY, PB-T50-RS, and ModelNet40, respectively. This indicates that simply applying Mamba to SNNs is insufficient. Additionally, both Model

SSM Branch		OBJ-BG	PB-T50-RS	ModelNet40
Token Flip	Time Flip			
✗	✗	88.9	83.5	91.6
✓	✗	89.6	83.7	91.7
✓	✓	89.2	83.4	91.6
✗	✓	90.2	84.2	92.3

Table 5. Ablation study of the bidirectional strategy. We report overall accuracy (%) on OBJ-BG, PB-T50-RS and ModelNet40.

II and Model III outperform Model I, highlighting the effectiveness of the two SNN-adaptive branches. With these branches, SMB performs similarly to Mamba while reducing energy consumption.

Bidirectional Strategy In Tab. 5, we further evaluate the impact of two bidirectional strategies. Token Flip reverses the token dimension, while Time Flip reverses the time dimension. When neither is used, SSM branch degenerates into unidirectional SSM leading to poor performance. Using only Token Flip performs better than unidirectional SSM, but reflects a 0.4%, 0.4%, and 0.3% drop in OA compared to Time Flip. Additionally, applying both strategies degrades performance to that of unidirectional SSM. These results highlight the critical role of bidirectional strategies in SMB. Specifically, Time Flip proves more effective than

HDE		OBJ-BG	PB-T50-RS	ModelNet40
Forward	Backward			
✗	✗	88.6	83.7	91.5
✗	✓	89.8	83.8	92.0
✓	✗	89.5	84.0	91.7
✓	✓	90.2	84.2	92.3

Table 6. Ablation study of encoding method performance. We report overall accuracy (%) on OBJ-BG, PB-T50-RS and ModelNet40. Forward denotes *finite forward sliding* while Backward denotes *infinite backward extension*.

Timestep	Energy(mJ)	OBJ-BG	PB-T50-RS	ModelNet40
ANN	18.9	90.2	85.4	92.4
1	1.5	88.9	83.3	91.6
2	2.8	89.8	83.7	91.8
3	3.9	90.2	83.8	92.1
4	5.4	90.2	84.2	92.3
6	7.6	90.0	84.3	92.3

Table 7. Ablation study of time step. We report overall accuracy (%) and Energy(mJ) on OBJ-BG, PB-T50-RS and ModelNet40. ANN refers to PointMamba.

Token Flip in enabling the network to capture more meaningful interaction. However, the combination of both strategies hinders model performance, likely due to the limited information in the spike input to SSM.

5.3.2. Ablation on HDE

As shown in Tab. 6, we evaluate the impact of *finite forward sliding* and *infinite backward extension* of HDE on the OBJ-BG, PB-T50-RS and ModelNet40 datasets. When both are applied simultaneously, SPM achieves the best performance on all datasets, with 90.2%, 84.2%, and 92.3% OA respectively. Conversely, when neither of them is used, HDE degenerates into direct encoding, reflecting a relative decline in performance. Furthermore, the performance also improves when either of them is used individually. This means that both *finite forward sliding* and *infinite backward extension* contribute effectively to model performance.

5.3.3. Ablation on Time Step

In Tab. 7, we further evaluate SPM’s performance and energy consumption on OBJ-BG, PB-T50-RS and ModelNet40 under different time steps, including PointMamba as ANN counterpart for comparison. Given the high computational cost, the maximum time step is set to 6.

Unlike previous works [42, 54], we can see that in Tab. 7, SPM’s performance improves with time steps, plateauing at 4 and 6 with 90.2%, 84.3%, and 92.3% OA, respectively. This suggests that by introducing temporal dynamics and leveraging SNNs’ time feature extraction, SPM alleviates the redundancy of direct encoding in point cloud analy-

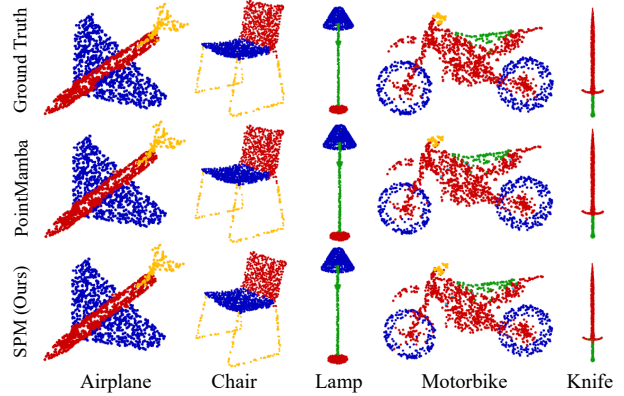


Figure 4. Qualitative results of part segmentation of our SPM and ANN counterpart (PointMamba) on ShapeNetPart.

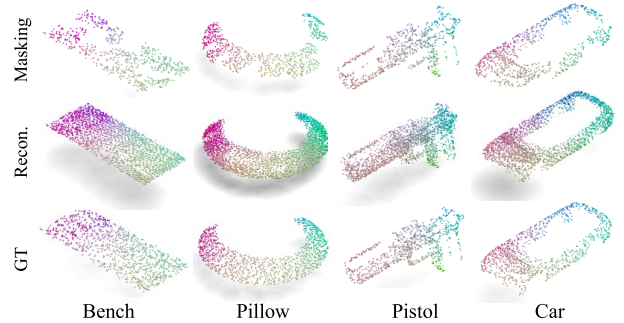


Figure 5. Qualitative results of reconstruction on ShapeNet.

sis [54]. Meanwhile, SPM achieves a $12.6\times$ energy reduction over PointMamba at 1 time step and $3.5\times$ at 4 time steps while maintaining comparable performance.

5.4. Visualizations

We visualize part segmentation results of SPM and its ANN counterpart, PointMamba, in Fig. 4. The segmentation visualizations of SPM are nearly identical to PointMamba, with minor differences in fine details, while overall quality remains intact. Additionally, we present reconstruction visualizations of the pre-training in Fig. 5. Despite the high masking ratio, SPM effectively reconstructs the overall object shape. More visualizations can be seen in Appendix D.

6. Conclusion

In this work, we present Spiking Point Mamba (SPM), a novel SNN framework based on Mamba architecture for point cloud analysis. The proposed HDE and SMB effectively introduce temporal dynamics and utilize the modeling capacity of Mamba and SNNs, achieving a remarkable performance improvement in the SNN domain. We hope that SPM can further reduce energy consumption in future research for neuromorphic hardware deployment.

References

- [1] Romain Brette and Wulfram Gerstner. Adaptive exponential integrate-and-fire model as an effective description of neuronal activity. *Journal of neurophysiology*, 94(5):3637–3642, 2005. 5, 2
- [2] Tong Bu, Wei Fang, Jianhao Ding, PengLin Dai, Zhaofei Yu, and Tiejun Huang. Optimal ann-snn conversion for high-accuracy and ultra-low-latency spiking neural networks. *arXiv preprint arXiv:2303.04347*, 2023. 2
- [3] Adi R Bulsara, Tim C Elston, Charles R Doering, Steve B Lowen, and Katja Lindenberg. Cooperative behavior in periodically driven noisy integrate-fire models of neuronal dynamics. *Physical Review E*, 53(4):3958, 1996. 2
- [4] Angel X Chang, Thomas Funkhouser, Leonidas Guibas, Pat Hanrahan, Qixing Huang, Zimo Li, Silvio Savarese, Manolis Savva, Shuran Song, Hao Su, et al. Shapenet: An information-rich 3d model repository. *arXiv preprint arXiv:1512.03012*, 2015. 5
- [5] Tri Dao and Albert Gu. Transformers are ssms: Generalized models and efficient algorithms through structured state space duality. *arXiv preprint arXiv:2405.21060*, 2024. 2
- [6] Mehmet Hamza Erol, Arda Senocak, Jiu Feng, and Joon Son Chung. Audio mamba: Bidirectional state space model for audio representation learning. *IEEE Signal Processing Letters*, 2024. 2
- [7] Wei Fang, Zhaofei Yu, Yanqi Chen, Timothée Masquelier, Tiejun Huang, and Yonghong Tian. Incorporating learnable membrane time constant to enhance learning of spiking neural networks. In *Proceedings of the IEEE/CVF international conference on computer vision*, pages 2661–2671, 2021. 2
- [8] Daniel Y Fu, Tri Dao, Khaled Kamal Saab, Armin W Thomas, Atri Rudra, and Christopher Re. Hungry hungry hippos: Towards language modeling with state space models. In *The Eleventh International Conference on Learning Representations*, 2023. 2
- [9] Wulfram Gerstner and Werner M Kistler. *Spiking neuron models: Single neurons, populations, plasticity*. Cambridge university press, 2002. 2
- [10] Karan Goel, Albert Gu, Chris Donahue, and Christopher Ré. It’s raw! audio generation with state-space models. In *International conference on machine learning*, pages 7616–7633. PMLR, 2022. 2
- [11] Albert Gu and Tri Dao. Mamba: Linear-time sequence modeling with selective state spaces. *arXiv preprint arXiv:2312.00752*, 2023. 1, 2
- [12] Albert Gu and Tri Dao. Mamba: Linear-time sequence modeling with selective state spaces. In *First Conference on Language Modeling*, 2024. 2
- [13] Albert Gu, Karan Goel, and Christopher Ré. Efficiently modeling long sequences with structured state spaces. *arXiv preprint arXiv:2111.00396*, 2021. 2
- [14] Albert Gu, Karan Goel, Ankit Gupta, and Christopher Ré. On the parameterization and initialization of diagonal state space models. *Advances in Neural Information Processing Systems*, 35:35971–35983, 2022. 2
- [15] Albert Gu, Isys Johnson, Aman Timalina, Atri Rudra, and Christopher Re. How to train your hippo: State space models with generalized orthogonal basis projections. In *International Conference on Learning Representations*, 2023. 2
- [16] Yufei Guo, Xiaode Liu, Yuanpei Chen, Liwen Zhang, Weihang Peng, Yuhan Zhang, Xuhui Huang, and Zhe Ma. Rmp-loss: Regularizing membrane potential distribution for spiking neural networks. In *Proceedings of the IEEE/CVF International Conference on Computer Vision*, pages 17391–17401, 2023. 2
- [17] Ankit Gupta, Albert Gu, and Jonathan Berant. Diagonal state spaces are as effective as structured state spaces. *Advances in Neural Information Processing Systems*, 35:22982–22994, 2022. 2
- [18] Xu Han, Yuan Tang, Zhaoxuan Wang, and Xianzhi Li. Mamba3d: Enhancing local features for 3d point cloud analysis via state space model. In *Proceedings of the 32nd ACM International Conference on Multimedia*, pages 4995–5004, 2024. 1, 5
- [19] Zecheng Hao, Tong Bu, Jianhao Ding, Tiejun Huang, and Zhaofei Yu. Reducing ann-snn conversion error through residual membrane potential. In *Proceedings of the AAAI conference on artificial intelligence*, pages 11–21, 2023. 2
- [20] Yangfan Hu, Qian Zheng, Xudong Jiang, and Gang Pan. Fast-snn: fast spiking neural network by converting quantized ann. *IEEE Transactions on Pattern Analysis and Machine Intelligence*, 2023. 2
- [21] Yuxiang Lan, Yachao Zhang, Xu Ma, Yanyun Qu, and Yun Fu. Efficient converted spiking neural network for 3d and 2d classification. In *Proceedings of the IEEE/CVF International Conference on Computer Vision*, pages 9211–9220, 2023. 6
- [22] Kunchang Li, Xinhao Li, Yi Wang, Yanan He, Yali Wang, Limin Wang, and Yu Qiao. Videomamba: State space model for efficient video understanding. In *European Conference on Computer Vision*, pages 237–255. Springer, 2024. 2
- [23] Lei Li, Siyu Zhu, Hongbo Fu, Ping Tan, and Chiew-Lan Tai. End-to-end learning local multi-view descriptors for 3d point clouds. In *Proceedings of the IEEE/CVF conference on computer vision and pattern recognition*, pages 1919–1928, 2020. 2
- [24] Dingkan Liang, Xin Zhou, Wei Xu, Xingkui Zhu, Zhikang Zou, Xiaoqing Ye, Xiao Tan, and Xiang Bai. Pointmamba: A simple state space model for point cloud analysis. *Advances in neural information processing systems*, 37:32653–32677, 2025. 1, 2, 5, 6
- [25] Haotian Liu, Mu Cai, and Yong Jae Lee. Masked discrimination for self-supervised learning on point clouds. In *ECCV*, 2022. 6
- [26] Jiuming Liu, Jinru Han, Lihao Liu, Angelica I Aviles-Rivero, Chaokang Jiang, Zhe Liu, and Hesheng Wang. Mamba4d: Efficient long-sequence point cloud video understanding with disentangled spatial-temporal state space models. *arXiv preprint arXiv:2405.14338*, 2024. 2
- [27] Jiuming Liu, Ruiji Yu, Yian Wang, Yu Zheng, Tianchen Deng, Weicai Ye, and Hesheng Wang. Point mamba: A novel point cloud backbone based on state space model with octree-based ordering strategy. *arXiv preprint arXiv:2403.06467*, 2024. 2
- [28] Yue Liu, Yunjie Tian, Yuzhong Zhao, Hongtian Yu, Lingxi Xie, Yaowei Wang, Qixiang Ye, Jianbin Jiao, and Yunfan

- Liu. Vmamba: Visual state space model. *Advances in neural information processing systems*, 37:103031–103063, 2025. 2
- [29] Xinhao Luo, Man Yao, Yuhong Chou, Bo Xu, and Guoqi Li. Integer-valued training and spike-driven inference spiking neural network for high-performance and energy-efficient object detection. In *European Conference on Computer Vision*, pages 253–272. Springer, 2024. 2
- [30] Xu Ma, Can Qin, Haoxuan You, Haoxi Ran, and Yun Fu. Rethinking network design and local geometry in point cloud: A simple residual mlp framework. In *International Conference on Learning Representations*, 2022. 2, 6
- [31] Daniel Maturana and Sebastian Scherer. Voxnet: A 3d convolutional neural network for real-time object recognition. In *2015 IEEE/RSJ international conference on intelligent robots and systems (IROS)*, pages 922–928. IEEE, 2015. 2
- [32] Harsh Mehta, Ankit Gupta, Ashok Cutkosky, and Behnam Neyshabur. Long range language modeling via gated state spaces. In *The Eleventh International Conference on Learning Representations*, 2023. 2
- [33] Eric Nguyen, Karan Goel, Albert Gu, Gordon Downs, Preey Shah, Tri Dao, Stephen Baccus, and Christopher Ré. S4nd: Modeling images and videos as multidimensional signals with state spaces. *Advances in neural information processing systems*, 35:2846–2861, 2022. 2
- [34] Antonio Orvieto, Samuel L Smith, Albert Gu, Anushan Fernando, Caglar Gulcehre, Razvan Pascanu, and Soham De. Resurrecting recurrent neural networks for long sequences. In *International Conference on Machine Learning*, pages 26670–26698. PMLR, 2023. 2
- [35] Hanyu Ouyang and Jie Jiang. Spiking-detr: A spike-driven end-to-end object detection framework on spike-form data streams using spiking-transformer and spiking residual learning. *Available at SSRN 4706194*, 2024. 1, 2
- [36] Yatian Pang, Wenxiao Wang, Francis EH Tay, Wei Liu, Yonghong Tian, and Li Yuan. Masked autoencoders for point cloud self-supervised learning. In *ECCV*, 2022. 6
- [37] Chunghyun Park, Yoonwoo Jeong, Minsu Cho, and Jaesik Park. Fast point transformer. In *Proceedings of the IEEE/CVF conference on computer vision and pattern recognition*, pages 16949–16958, 2022. 2
- [38] Anh Viet Phan, Minh Le Nguyen, Yen Lam Hoang Nguyen, and Lam Thu Bui. Dgcnn: A convolutional neural network over large-scale labeled graphs. *Neural Networks*, 108:533–543, 2018. 6
- [39] Charles R Qi, Hao Su, Kaichun Mo, and Leonidas J Guibas. Pointnet: Deep learning on point sets for 3d classification and segmentation. In *Proceedings of the IEEE conference on computer vision and pattern recognition*, pages 652–660, 2017. 2, 6
- [40] Charles Ruizhongtai Qi, Li Yi, Hao Su, and Leonidas J Guibas. Pointnet++: Deep hierarchical feature learning on point sets in a metric space. *Advances in neural information processing systems*, 30, 2017. 2, 6
- [41] Xuerui Qiu, Man Yao, Jieyuan Zhang, Yuhong Chou, Ning Qiao, Shibo Zhou, Bo Xu, and Guoqi Li. Efficient 3d recognition with event-driven spike sparse convolution. *arXiv preprint arXiv:2412.07360*, 2024. 1, 2
- [42] Dayong Ren, Zhe Ma, Yuanpei Chen, Weihang Peng, Xiaode Liu, Yuhan Zhang, and Yufei Guo. Spiking pointnet: Spiking neural networks for point clouds. *Advances in Neural Information Processing Systems*, 36, 2024. 1, 6, 8
- [43] Kaushik Roy, Akhilesh Jaiswal, and Priyadarshini Panda. Towards spike-based machine intelligence with neuromorphic computing. *Nature*, 575(7784):607–617, 2019. 1
- [44] Catherine D Schuman, Shruti R Kulkarni, Maryam Parsa, J Parker Mitchell, Bill Kay, et al. Opportunities for neuromorphic computing algorithms and applications. *Nature Computational Science*, 2(1):10–19, 2022. 1
- [45] Sara Sedighi, Farhana Afrin, Elonna Onyejebu, and Kurtis D Cantley. Visual analysis of leaky integrate-and-fire spiking neuron models and circuits. In *2024 IEEE 67th International Midwest Symposium on Circuits and Systems (MWSCAS)*, pages 1437–1440. IEEE, 2024. 2
- [46] Shuaijie Shen, Chao Wang, Renzhuo Huang, Yan Zhong, Qinghai Guo, Zhichao Lu, Jianguo Zhang, and Luziwei Leng. Spikingssms: Learning long sequences with sparse and parallel spiking state space models. *arXiv preprint arXiv:2408.14909*, 2024. 2
- [47] Shaoshuai Shi, Chaoxu Guo, Li Jiang, Zhe Wang, Jianping Shi, Xiaogang Wang, and Hongsheng Li. Pv-rcnn: Point-voxel feature set abstraction for 3d object detection. In *Proceedings of the IEEE/CVF conference on computer vision and pattern recognition*, pages 10529–10538, 2020. 2
- [48] Jimmy TH Smith, Andrew Warrington, and Scott Linderman. Simplified state space layers for sequence modeling. In *The Eleventh International Conference on Learning Representations*, 2023. 2
- [49] Mikaela Angelina Uy, Quang-Hieu Pham, Binh-Son Hua, Thanh Nguyen, and Sai-Kit Yeung. Revisiting point cloud classification: A new benchmark dataset and classification model on real-world data. In *Proceedings of the IEEE/CVF international conference on computer vision*, pages 1588–1597, 2019. 5
- [50] Ziqing Wang, Yuetong Fang, Jiahang Cao, Qiang Zhang, Zhongrui Wang, and Renjing Xu. Masked spiking transformer. In *Proceedings of the IEEE/CVF International Conference on Computer Vision*, pages 1761–1771, 2023. 2
- [51] Chengzhi Wu, Junwei Zheng, Julius Pfommer, and Jürgen Beyerer. Attention-based point cloud edge sampling. In *CVPR*, 2023. 6
- [52] Peixi Wu, Bosong Chai, Hebei Li, Menghua Zheng, Yansong Peng, Zeyu Wang, Xuan Nie, Yueyi Zhang, and Xiaoyan Sun. Spiking point transformer for point cloud classification, 2025. 6
- [53] Qiaoyun Wu, Quanxiao Zhang, Chunyu Tan, Yun Zhou, and Changyin Sun. Point-to-spike residual learning for energy-efficient 3d point cloud classification. In *Proceedings of the AAAI Conference on Artificial Intelligence*, pages 6092–6099, 2024. 1, 2
- [54] Qiaoyun Wu, Quanxiao Zhang, Chunyu Tan, Yun Zhou, and Changyin Sun. Point-to-spike residual learning for energy-efficient 3d point cloud classification. In *Proceedings of the AAAI Conference on Artificial Intelligence*, pages 6092–6099, 2024. 6, 8

- [55] Xiaoyang Wu, Yixing Lao, Li Jiang, Xihui Liu, and Hengshuang Zhao. Point transformer v2: Grouped vector attention and partition-based pooling. *Advances in Neural Information Processing Systems*, 35:33330–33342, 2022. [2](#)
- [56] Zhirong Wu, Shuran Song, Aditya Khosla, Fisher Yu, Linguang Zhang, Xiaoou Tang, and Jianxiong Xiao. 3d shapenets: A deep representation for volumetric shapes. In *Proceedings of the IEEE conference on computer vision and pattern recognition*, pages 1912–1920, 2015. [5](#)
- [57] Yijun Yang, Zhaohu Xing, Lequan Yu, Chunwang Huang, Huazhu Fu, and Lei Zhu. Vivim: A video vision mamba for medical video segmentation. *arXiv preprint arXiv:2401.14168*, 2024. [2](#)
- [58] Man Yao, Jiakui Hu, Zhaokun Zhou, Li Yuan, Yonghong Tian, Bo Xu, and Guoqi Li. Spike-driven transformer. *Advances in neural information processing systems*, 36, 2024. [2](#)
- [59] Li Yi, Vladimir G Kim, Duygu Ceylan, I-Chao Shen, Mengyan Yan, Hao Su, Cewu Lu, Qixing Huang, Alla Sheffer, and Leonidas Guibas. A scalable active framework for region annotation in 3d shape collections. *ACM Transactions on Graphics (ToG)*, 35(6):1–12, 2016. [5](#)
- [60] Nan Yin, Mengzhu Wang, Zhenghan Chen, Giulia De Masi, Huan Xiong, and Bin Gu. Dynamic spiking graph neural networks. In *Proceedings of the AAAI Conference on Artificial Intelligence*, pages 16495–16503, 2024. [2](#)
- [61] Xumin Yu, Lulu Tang, Yongming Rao, Tiejun Huang, Jie Zhou, and Jiwen Lu. Point-bert: Pre-training 3d point cloud transformers with masked point modeling. In *Proceedings of the IEEE/CVF conference on computer vision and pattern recognition*, pages 19313–19322, 2022. [6](#)
- [62] Guowen Zhang, Lue Fan, Chenhang He, Zhen Lei, Zhaoxiang Zhang, and Lei Zhang. Voxel mamba: Group-free state space models for point cloud based 3d object detection. *arXiv preprint arXiv:2406.10700*, 2024. [2](#)
- [63] Renrui Zhang, Ziyu Guo, Peng Gao, Rongyao Fang, Bin Zhao, Dong Wang, Yu Qiao, and Hongsheng Li. Point-m2ae: multi-scale masked autoencoders for hierarchical point cloud pre-training. In *NeurIPS*, 2022. [6](#)
- [64] Shimin Zhang, Qu Yang, Chenxiang Ma, Jibin Wu, Haizhou Li, and Kay Chen Tan. Tc-lif: A two-compartment spiking neuron model for long-term sequential modelling. In *Proceedings of the AAAI Conference on Artificial Intelligence*, pages 16838–16847, 2024. [2](#)
- [65] Tao Zhang, Haobo Yuan, Lu Qi, Jiangning Zhang, Qianyu Zhou, Shunping Ji, Shuicheng Yan, and Xiangtai Li. Point cloud mamba: Point cloud learning via state space model. *arXiv preprint arXiv:2403.00762*, 2024. [2](#)
- [66] Yan Zhong, Ruoyu Zhao, Chao Wang, Qinghai Guo, Jianguo Zhang, Zhichao Lu, and Luziwei Leng. Spike-ssm: A sparse, precise, and efficient spiking state space model for long sequences learning. *arXiv preprint arXiv:2410.17268*, 2024. [1](#), [2](#)
- [67] Chenlin Zhou, Han Zhang, Zhaokun Zhou, Liutao Yu, Liwei Huang, Xiaopeng Fan, Li Yuan, Zhengyu Ma, Huihui Zhou, and Yonghong Tian. Qkformer: Hierarchical spiking transformer using qk attention. *arXiv preprint arXiv:2403.16552*, 2024. [1](#)
- [68] Zhaokun Zhou, Kaiwei Che, Wei Fang, Keyu Tian, Yuesheng Zhu, Shuicheng Yan, Yonghong Tian, and Li Yuan. Spikformer v2: Join the high accuracy club on imagenet with an snn ticket. *arXiv preprint arXiv:2401.02020*, 2024. [1](#), [2](#)
- [69] Lianghui Zhu, Bencheng Liao, Qian Zhang, Xinlong Wang, Wenyu Liu, and Xinggang Wang. Vision mamba: Efficient visual representation learning with bidirectional state space model. In *Forty-first International Conference on Machine Learning*, 2024. [2](#)



Supplementary Material

In the supplementary material, we further explore the behavior of Farthest Point Sampling (FPS) and experimentally validate the theoretical foundation of HDE. We present more ablation studies on neurons and mask ratios, as well as comparing our SPM with additional models [41]. Next, we provide more implementation details of our SPM. Finally, we include additional visualizations across various tasks.

A. Farthest Point Sampling Behavior

Farthest Point Sampling (FPS) is a widely used technique for point cloud analysis, which select a subset of points from a larger point cloud in a way that maximizes the minimum distance between selected points. FPS can be divided into three key stages: early, middle, and late stages.

Early Stage. The early stage of FPS involves random initial selection, which can cause instability in the sampling process. The points selected in this stage are heavily influenced by the random choice, leading to a not so well distribution across the point cloud. This randomness results in high variance, making the early stage less reliable for capturing the overall structure of the point cloud. Together, the early stage is unstable due to random initial selection.

Middle Stage. As the algorithm progresses, the middle stage becomes more stable. FPS starts to cover important features of the geometry, improving the distribution of sampled points. The algorithm focuses on regions with significant features while maintaining a good spread across the point cloud. This stability enables a more meaningful representation of the point cloud. Together, the middle stage stabilizes and captures the skeletal structure.

Late Stage. In the late stage, FPS starts to experience diminishing returns. As the number of selected points increases, the algorithm starts to introduce redundancy or noise. The points selected in this stage are often located in areas that are already well-represented by previous selections, leading to overlapping regions. Together, the late stage may introduce redundancy or noise.

We use Chamfer Distance to measure the similarity between the early, middle, and late stages under different random seeds in Tab. 9, and visualize the sampling structures of the early, middle, and late stages under certain random seeds for quantitative comparison in Fig. 6, thereby demonstrating the rationale behind the hierarchical stages.

From Fig. 6, we can see that in the early stage under different random seeds, FPS is unstable and does not fully represent the object information, indicating a strong influence from the random initial points. In the middle stage,

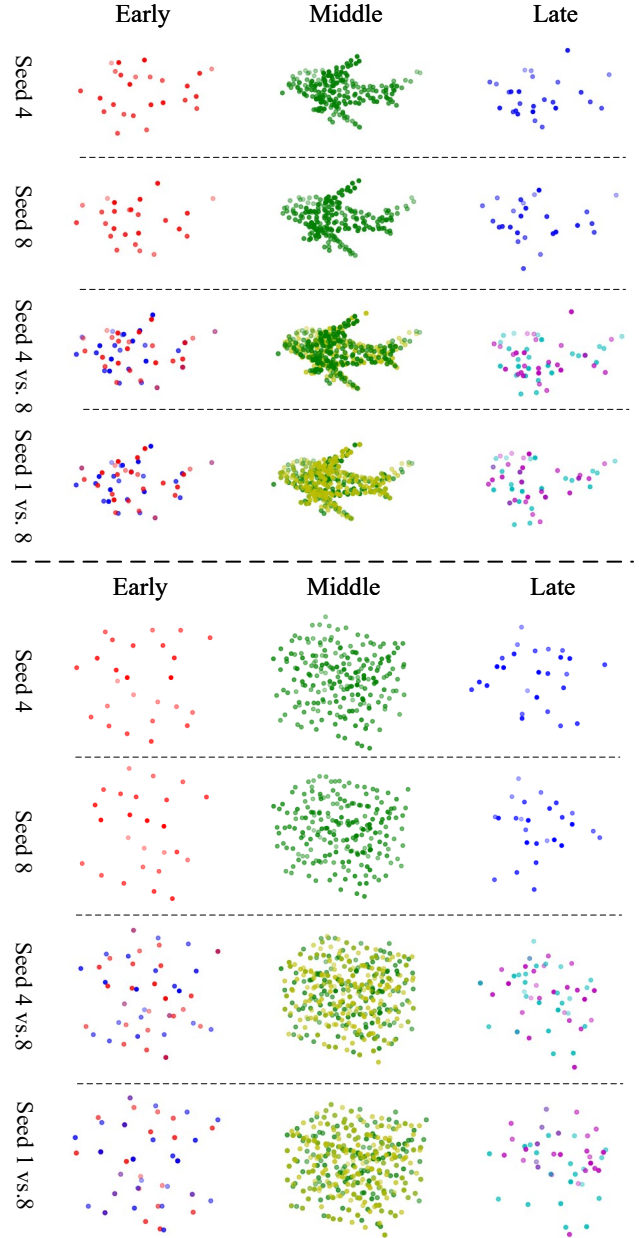


Figure 6. Quantitative comparison of the sampling structures of the early, middle, and late stages under different random seeds.

the points show little visual change and provide a stable representation of the entire point cloud. However, in the late stage, the point cloud no longer captures the overall

Configuration	Pre-training	Classification		Segmentation
	ShapeNet	ModelNet40	ScanObjectNN	ShapeNetPart
Optimizer	AdamW	AdamW	AdamW	AdamW
Learning rate	1e-3	1e-3	1e-3	2e-4
Weight decay	5e-2	5e-2	5e-2	5e-2
Learning rate scheduler	cosine	cosine	cosine	cosine
Training epochs	300	300	300	300
Warmup epochs	20	30	30	20
Batch size	128	72	36	36
Num. of encoder layers N	12	12	12	12
Num. of decoder layers N_d	4	-	-	-
Input points M	1024	1024	2048	2048
Num. of patches n	128	128	256	256
Patch size k	32	32	32	32
Augmentation	Scale&Trans	Scale&Trans	Rotation	-

Table 8. Implementation details for pre-training and downstream tasks such as classification and segmentation tasks.

structure, exhibiting a highly variable shape, and can only be considered as redundant points.

From Tab. 9, we can observe that the Chamfer Distance between the early, middle, and late stage point clouds under different random seeds can also be understood as their similarity. Multiple experiments indicate that the early and late stage points exhibit more unstable distributions compared to the middle stage points, which can be intuitively seen from the visualization in Fig. 6. Furthermore, the middle stage points show a high similarity across different random seeds, confirming that they reliably represent the skeletal structure of the entire point cloud. Additionally, we observe that the similarity between the late and middle stage points is also high, suggesting an overlap between these two stages and further supporting the redundancy characteristic of the late stage points.

B. Ablation Study

The ablation study mainly supplements performance comparison experiments for SPM with different neurons, as well as comparisons with other models [41] using ILIF [29] and its training strategies. Additionally, we conduct an ablation study on the pre-training mask ratio.

Ablation on different neurons. In Tab. 10, we conduct a detailed ablation study using different neurons on the OBJ-BG, OBJ-ONLY, PB-T50-RS and ModelNet40 datasets. It can be observed that the accuracy of traditional IF neurons and their variants tends to fluctuate only slightly, whereas ILIF significantly improves the model’s performance. This improvement is due to its integer-based training and spike-based inference mechanism. Therefore, a direct comparison with the traditional LIF model is not entirely reasonable. Here, we present the experimental results of SPM us-

Seed	Chamfer Distance			
	$D^{Early,Early}$	$D^{Mid,Mid}$	$D^{Mid,Late}$	$D^{Late,Late}$
1 vs. 2	0.18	0.09	0.11	0.24
4 vs. 7	0.17	0.07	0.09	0.20
6 vs. 25	0.16	0.06	0.08	0.22
16 vs. 32	0.19	0.06	0.10	0.25
44 vs. 42	0.18	0.06	0.10	0.22
123 vs. 321	0.19	0.06	0.07	0.23
<i>Mean</i>	0.18	0.07	0.09	0.23

Table 9. The similarity of the early, middle, and late stages under different random seeds. (a vs. b , $D^{A,B}$) denotes the Chamfer distance between stage A under random seed a and stage B under random seed b .

Method	Neurons	ScanObjectNN			ModelNet40
		OBJ-BG	OBJ-ONLY	PB-T50-RS	
E-3DSNN	ILIF [29]	86.5*	86.0*	80.4*	91.7
SPM	IF [3]	89.8	89.0	84.1	92.0
	LIF [9]	90.2	89.5	84.2	92.3
	EIF [1]	89.9	89.2	84.1	92.1
	PLIF [7]	90.5	89.6	84.1	92.5
	ILIF [29]	91.5	91.2	85.2	93.0
	<i>Improvement</i>	+5.0	+5.2	+4.8	+1.3

Table 10. Ablation study on different neurons with 4 time steps for IF, LIF, EIF and PLIF and 1×4 for ILIF.

ing ILIF, where accuracy reaches 91.5%, 91.2%, and 85.2% on OBJ-BG, OBJ-ONLY and PB-T50-RS datasets respectively, and 93.0% on the ModelNet40 dataset.

Comparison with other models. In Tab. 10, we also make an additional comparison between SPM and other ILIF-based models such as E-3DSNN. To ensure a fair comparison, we used a configuration of $T \times D$ as 1×4 , which follows the ILIF training strategy, allowing the model to

Masking ratio	Loss	PB-T50-RS	ModelNet40
0.4	1.66	86.1	92.6
0.6	1.57	86.5	93.1
0.8	2.03	85.9	92.7
0.9	2.00	86.0	92.5

Table 11. Ablation study on masking strategy. The pre-training loss ($\times 1000$) along with fine-tuning accuracy (%) are reported on PB-T50-RS and ModelNet40.

convert into 4 time steps for spike-based inference during the inference phase. In the case of using ILIF equally, we observe that our SPM significantly outperforms benchmark models such as E-3DSNN, with overall accuracy reaching 91.5%, 91.2%, 85.2%, and 93.0% on OBJ-BG, OBJ-ONLY, PB-T50-RS, and ModelNet40, respectively.

Ablation on mask ratios In Tab. 11, we conduct a detailed ablation study on the masking ratio. It can be observed that when the masking ratio is set to 0.6, which is the ratio we ultimately selected, the accuracy of the fine-tuning task reaches their optimal performance, outperforming other settings. This suggests that for spike-based pre-training, too much masking can lead to excessive information loss, preventing the SNN encoder from learning meaningful feature representations. On the other hand, too little masking may reduce the difficulty of the reconstruction task, also causing SNN encoder to fail to learn strong feature representations.

C. Implement details

In this section, we provide more specific details about the training parameters for each dataset, as shown in Tab. 8. Different training hyperparameters were used for different datasets, but the backbone remained the same, consisting of a 12-layer stacked SPM, which facilitated the generalization across different datasets and the fine-tuning of pre-training models.

D. More Visualizations

The figure of main paper shows only a few sample visualizations. In this section, we provide more visualizations to quantitatively demonstrate the effectiveness and performance of our SPM, as shown in Fig. 7 and Fig. 8.

As can be seen from Fig. 7, the part segmentation results of SPM are almost identical to those of PointMamba across different classes. Slightly more complex classes may show a minor difference, but it does not significantly affect the overall performance. From Fig. 8, it can also be observed that our SPM performs excellently in the pre-trained reconstruction task. Despite the large masking range, it is still able to recover the general shape of the object.

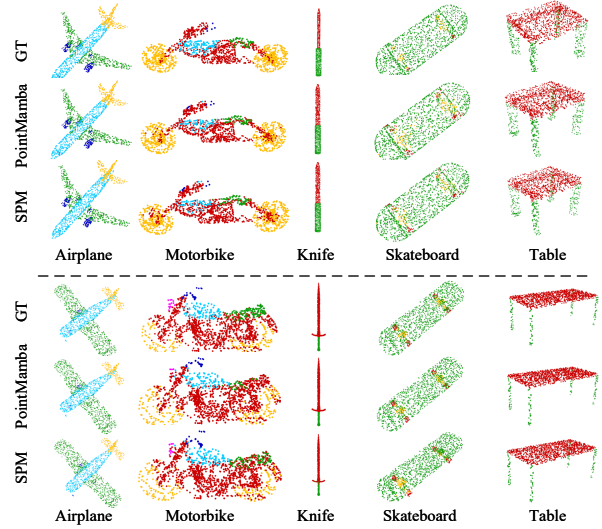


Figure 7. Qualitative results of part segmentation of our SPM and ANN counterpart (PointMamba) on ShapeNetPart.

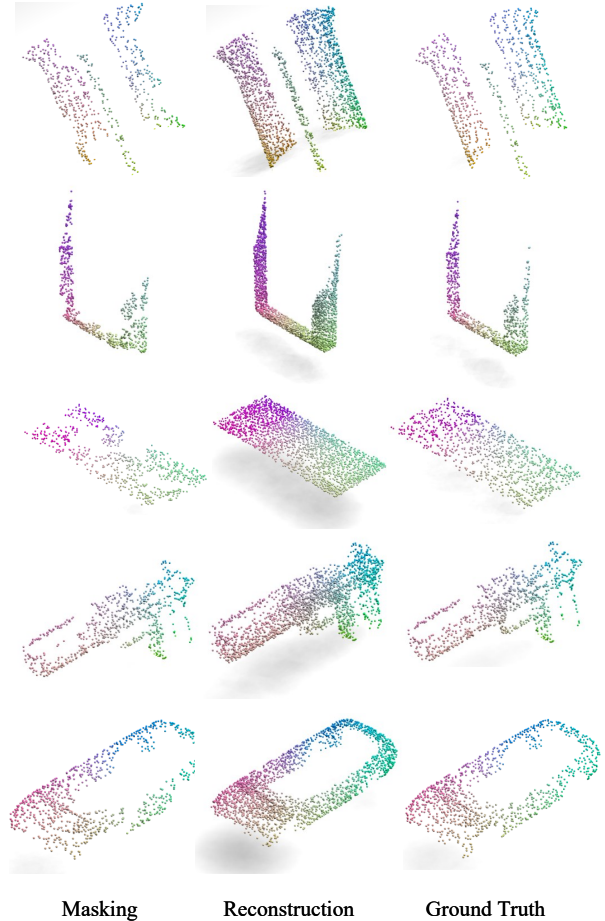


Figure 8. Qualitative results of reconstruction on ShapeNet.